Available online at www.sciencedirect.com
ScienceDirect
Trans. Nonferrous Met. Soc. China 25(2015) 1460−1467
Transactions of Nonferrous Metals Society of China
www.tnmsc.cn

Microstructural aspects of in-situ TiB reinforced Ti−6Al−4V composite processed by spark plasma sintering

Saeid GHESMATI TABRIZI[1], Abolfazl BABAKHANI[1], Seyed Abdolkarim SAJJADI[1], Wei-jie LÜ[2]

1. Department of Materials Science and Engineering, Engineering Faculty, Ferdowsi University of Mashhad, Mashhad 9177948974, Iran;
2. State Key Laboratory of Metal Matrix Composites, School of Materials Science and Engineering, Shanghai Jiao Tong University, Shanghai 200240, China

Received 6 June 2014; accepted 17 October 2014

Abstract: Titanium-matrix composites have important and wide applications in the transport and aerospace industries. The current research was focused on powder metallurgy processing of in-situ reinforced titanium-matrix composite with TiB whiskers. The Ti−6Al−4V alloy and B_4C additive powders were used as raw materials. Two different consolidation techniques, namely press-and-sintering and spark plasma sintering, were selected. It was observed that in-situ TiB whiskers were formed during sintering in both methods. The changes in size, aspect ratio and distribution of in-situ whiskers in different composite samples were monitored. The effect of spark plasma sintering temperature on the synthesis of in-situ whiskers was also investigated. Based on the microstructural observations (optical microscopy and scanning electron microscopy) and the energy dispersive spectroscopy analysis, it was concluded that increasing the spark plasma sintering temperature from 900 to 1100 °C would lead to the complete formation of in-situ TiB whiskers and reduced porosity content.

Key words: Ti−6Al−4V metal matrix composite; TiB whisker; in-situ reaction; spark plasma sintering

1 Introduction

Titanium alloys possess high corrosion resistance and high specific strength which are required for automotive, aerospace, and biomedical industries [1−3]. Powder metallurgy (PM) processes provide good opportunities both in cost reduction and microstructure enhancement [1,4]. PM process also benefits lower processing temperature compared with ingot metallurgy which inhibits microstructural coarsening of both the matrix and the reinforcements.

During the development of titanium-matrix composites (TMCs), different reinforcements including SiC fibers [5,6] and particles [7], carbon nano-tubes [8,9], TiB whiskers [10−12], TiB_2 [13] and TiC particles [14−16] and SiO_2 [17] were investigated. Some researchers concentrated on mechanical behavior of TMCs reinforced by both TiB whiskers (TiB_w) and TiC particles (TiC_p) which were produced by casting process [18]. It has been reported that TiB_w can undertake loads while TiC_p prevents crack formation and propagation in pure Ti-matrix composite [19]. In-situ TiB_w has high modulus of elasticity, hardness and chemical compatibility with Ti matrix. The clean interface of in-situ TiB_w provides strong bonds with Ti matrix [20]. In addition, coefficients of thermal expansion of TiB_w (7.2×10^{-6} °C^{-1}) and Ti-matrix (8.2×10^{-6} °C^{-1}) are compatible [21]. The in-situ reinforcements also have higher thermodynamic stability compared with ex-situ added reinforcements [22].

TiB_w is the in-situ product of the reaction between elemental boron, or its compounds, and titanium during solidification or sintering. The boron can be supplied from additive materials like TiB_2 [11,23], B_4C [24] or boron [25]. The reactions between titanium alloy and different additives are as follows:

$$Ti+TiB_2\rightarrow 2TiB \quad (1)$$

$$5Ti+B_4C\rightarrow 4TiB+TiC \quad (2)$$

$$Ti+B\rightarrow TiB \quad (3)$$

TiB has a *B*27 crystal structure and a more likely growth along [010] direction; hence, TiB reinforcements

Corresponding author: Saeid GHESMATI TABRIZI; Tel: +98-9153115255; E-mail: s_ghesmati@yahoo.com
DOI: 10.1016/S1003-6326(15)63746-3

obtain whisker-like morphology. The transverse section of TiB whiskers has hexagonal shape. The faceted interfaces between TiB_w and Ti matrix minimize the lattice strains [25−27].

Some PM processes like hot pressing and spark plasma sintering (SPS) apply heat and pressure simultaneously which is advantageous for removing the porosities. In SPS process, current pulses of high density (several thousand amperes) and voltages lower than 50 V are directly applied to the powder. Based on the microstructural observations, ZHANG et al [28] provided experimental proof that the DC on-off pulses cause plasma electric microdischarges between particles. When the particles contact each other, the electric discharges stop. Then joule heating and plastic deformation make the densification process proceed [28]. Another advantage of the SPS process is short sintering time compared with that of hot pressing or hot isostatic pressing [28,29]. Some researchers have studied the effect of SPS temperature on the remained porosities and the level of the progress of in-situ reactions. MORSI et al [24] studied the microstructure of Ti−TiB_2 mixture that was SPS processed. FENG et al [30] used the powder system Ti−B for SPS processing. They concluded that although the porosity content was reduced by increasing the SPS temperature, but TiB_w coarsened.

In this research work, the in-situ production of TiB reinforced Ti−6Al−4V alloy by conventional press-and-sintering and SPS process was investigated. The effects of processing type and SPS temperature on the completion of in-situ reaction were monitored. It aimed to obtain Ti−6Al−4V matrix composite material containing the least amount of un-reacted additive boron source. The changes in porosities and in-situ TiB_w reinforcements were also reported.

2 Experimental

The raw materials included alloy Ti−6Al−4V powder and B_4C powder. The average particle sizes of titanium and B_4C powders were <63 μm and 4−6 μm, respectively. The amount of B_4C powder was ranged between 0.12% and 0.48% (mass fraction). According to the stoichiometric calculations, it is equivalent to TiB_w content between 0.5% and 2% (volume fraction). The two powders were mixed in a jar mill using ceramic balls. The milling time was 2 h with the ball-to-powder mass ratio of 5:1. The mixed powders were consolidated by two different methods. The first method was based on press-and-sintering of the powders. Cold pressing was accomplished in a steel mold using a pressure of 420 MPa. Afterwards, the compacted specimens were sintered at 1250 °C for 150 min in a furnace with vacuum of 1×10^{-2} Pa.

In the second approach (SPS), powder mixture was inserted in a graphite die with an internal diameter of 50 mm and a height of 45 mm. A constant uniaxial pressure of 20 MPa was maintained on the powder mixture while DC on/off electric pulses were applied to the powder. The amount of powder was controlled so that the height of samples after SPS reached 10 mm. Two different sintering temperatures of 900 and 1100 °C were applied. The holding time for all samples was 10 min. Heating rates from room temperature to 750 °C and then to the sintering temperature were 100 and 25 °C/min, respectively. The chemical composition and processing parameters of the composite samples are indicated in Table 1.

Table 1 Processing parameters of titanium composite

Sample No.	Volume fraction of in-situ TiB/%[1)]	Processing type	Sintering temperature/ °C	Holding time/ min
PM1	1	CV	1250	150
PM2	2	CV	1250	150
L-SPS2	2	SPS	900	10
H-SPS0.5	0.5	SPS	1100	10
H-SPS1	1	SPS	1100	10
H-SPS2	2	SPS	1100	10

1) Stoichiometric prediction; CV: Cold pressing + vacuum sintering

All sintered samples were prepared for microstructure observation. The preparation consisted of wire-cutting, grinding, polishing, and etching with Kroll reagent. Microstructural observations of the composite samples were accomplished by optical microscopy (OM) and scanning electron microscopy (SEM).

The microstructure parameters including the length and diameter of TiB whiskers were measured using image analysis with Clemex software. They were made on several whiskers in different areas of each composite sample. Based on the measurements made on each whisker, the aspect ratio was calculated as the ratio of the length of the whiskers to their diameter. The average values are reported in the result section.

3 Results and discussion

3.1 Microstructure of cold pressed and sintered composites

The optical microstructures of Samples PM1 and PM2 are presented in Fig. 1. In-situ TiB_w is visible as gray needles. Titanium matrix consists of two phases of α (bright phase) and β (brown phase mostly at grain boundaries) as indicated in Fig. 1(b). Dark areas, which are round or elongated, represent the remained porosities after sintering. It should be mentioned that TiB_w found in the TMCs has the similar morphology with the

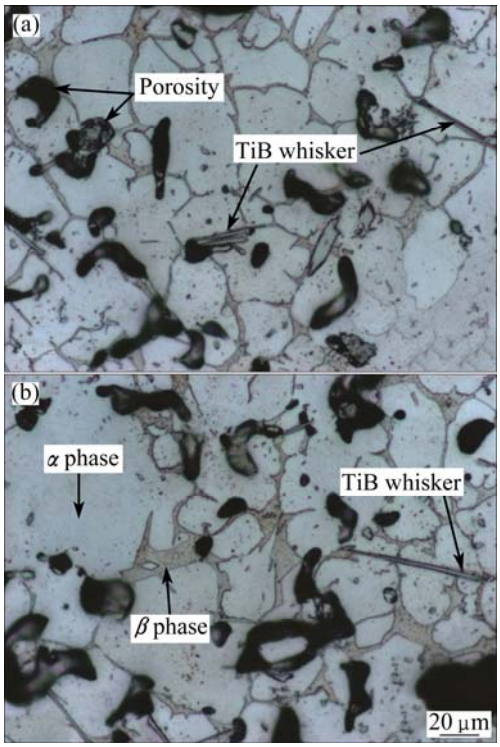

Fig. 1 OM microstructures of press-and-sintered samples: (a) Sample PM1; (b) Sample PM2

whiskers in cast [26] and extruded [31] TMCs.

There are some contents of porosities in the press-and-sintered composite samples (Figs. 1 and 2). It is believed that the remained porosities have an adverse effect on mechanical properties.

Higher magnification SEM image of one of the porosities in Sample PM1 is presented in Fig. 2(c). In addition, some clusters of TiB_w are present. They may be caused by the nucleation of multiple TiB whiskers near the previous B_4C particles. It is reported that whisker clusters act as stress concentration centers and crack nucleation sites [31].

The energy dispersive spectroscopy (EDS) point analysis was also conducted on several whiskers in TMC samples by SEM. The average B and Ti contents of whiskers in composite Samples PM1 and PM2 are presented in Table 2. The results confirm that both single and clustered whiskers are made of TiB.

Points *A* in Fig. 2(b) refer to TiB_w cut almost perpendicular to their longitudinal axis during sectioning of the sample. As can be seen, they possess hexagonal cross section shape which is in accordance with that reported in other works [30]. Some TiB whisker cuts parallel to the longitudinal axis are also marked in Fig. 2(b) (Points *B*).

Multiple measurements were made on the whiskers in press-and-sintered TMCs. The results show that the whiskers are 40−70 μm in length and 2−5 μm in thickness. The whiskers are formed with a wide range of

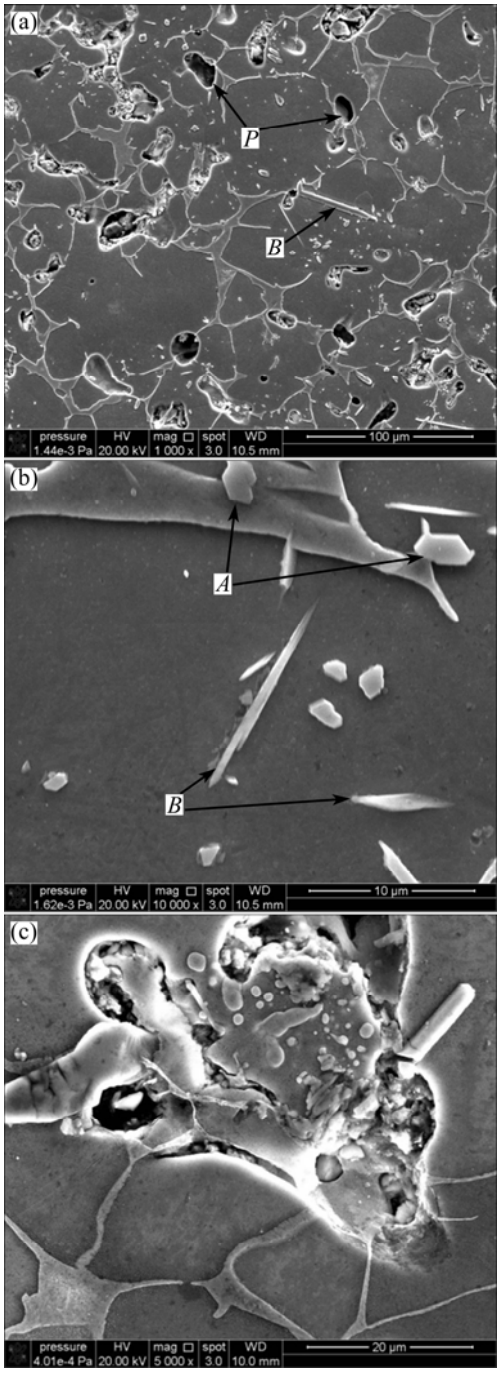

Fig. 2 SEM microstructures of press-and-sintered samples: (a) Two-phase α+β matrix of Sample PM2, in-situ TiB_w (Point *B*), and some porosities (Point *P*); (b) Transverse (Point *A*) and longitudinal (Point *B*) sections of some TiB_w in sample PM2; (c) TiB_w cluster in Sample PM1

Table 2 Average results of EDS analysis on some clustered and single whiskers

Element	Mass fraction/%	
	Single whisker	Clustered whisker
Ti	80	79
B	20	21

aspect ratios (8−20) which are caused by the high sintering temperature and long sintering time. The whiskers that nucleate earlier have more chance of growth. Since the growth rate in one crystal direction is more rapid than that in other directions, they obtained higher length and aspect ratio (comparing whiskers (Point *B*) in Fig. 2(a) with those in Fig. 2(b)).

3.2 Microstructure of spark plasma sintered composites

The OM images of Sample L-SPS2 (sintered at 900 °C) are presented in Fig. 3. The images corresponding to Sample H-SPS1 (sintered at 1100 °C) are presented in Fig. 4. These images were taken before etching the samples in order to observe only the in-situ reinforcements.

By comparing Figs. 3 and 4, it is noticed that equiaxed particles with the size of 6−10 μm are distributed in the matrix of Sample L-SPS2 while they are absent in Sample H-SPS1. These particles are the remainder of the B_4C additive particles that have not enough activation energy or time for decomposition. In-situ TiB whiskers with the average length of 20 μm are observed at higher magnification in Sample L-SPS2 (Fig. 3(b)). It is also obvious that porosities are removed by increasing sintering temperature from 900 to 1100 °C.

The OM microstructures of Samples L-SPS2 and H-SPS0.5 after etching are shown in Fig. 5. In both samples, the Widmanstatten plates of α phase are visible in the transformed β matrix.

The SEM observation of the composite sample L-SPS2 sintered at 900 °C confirms the presence of some few amounts of porosities (Fig. 6). There are no visible porosities in the TMCs sintered at 1100 °C (Fig. 7). As can be seen, the in-situ TiB_w is uniformly distributed in the titanium matrix of Sample H-SPS0.5.

The size measurements on TiB_w in TMCs produced by SPS reveal that the maximum length of whiskers in samples sintered at 900 °C is 15 μm. The in-situ whiskers in TMCs sintered at 1100 °C have different lengths in the range of 10−20 μm, although there are some larger whiskers with up to 50 μm in length which are the results of higher growth at higher temperatures. This is due to the fact that at higher temperatures, precipitates can grow more readily. The transverse sizes of whiskers are 1−2 μm. Hence, the maximum aspect ratio of the whiskers in Sample L-SPS2 is about 7:1 while in H-SPS TMCs it varies between 10:1 and 25:1. Compared with press-and-sintered samples PM1 and PM2, the aspect ratio of TiB_w in H-SPS samples is 20%

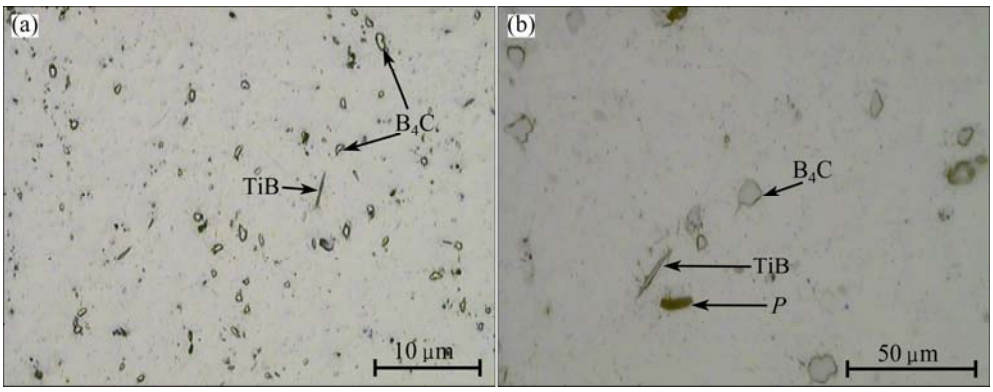

Fig. 3 As-polished OM images of composite sample L-SPS2 sintered at 900 °C: (a) Un-reacted B_4C particles dispersed in matrix; (b) In-situ TiB_w produced during sintering, remained B_4C particles and porosities (Point *P*)

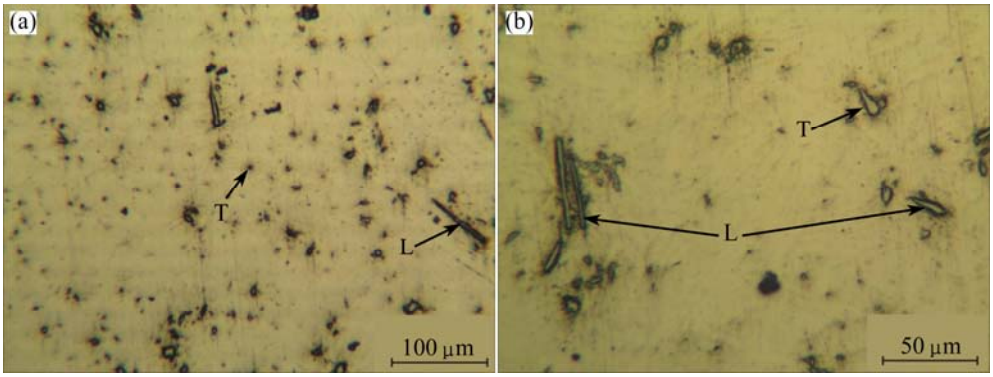

Fig. 4 As-polished OM images of composite sample H-SPS1 sintered at 1100 °C showing longitudinal (L) and transverse (T) sections of TiB whiskers

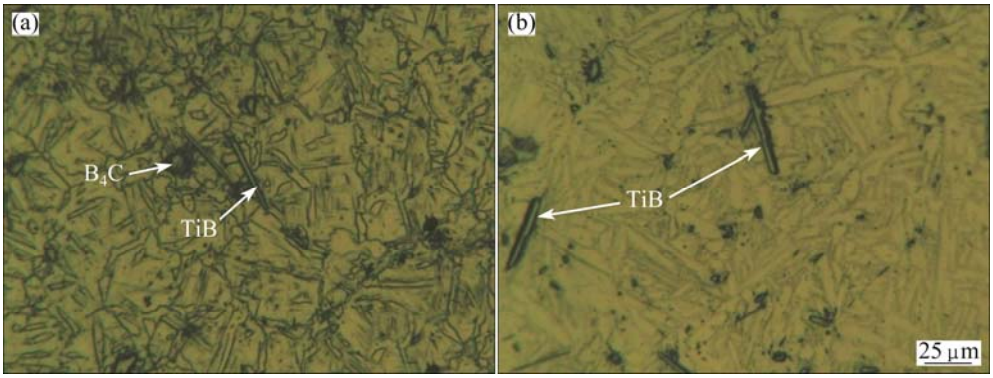

Fig. 5 OM images of composite samples after etching: (a) TiB_w and remained B_4C particles in Sample L-SPS2; (b) Some TiB_w in Sample H-SPS0.5

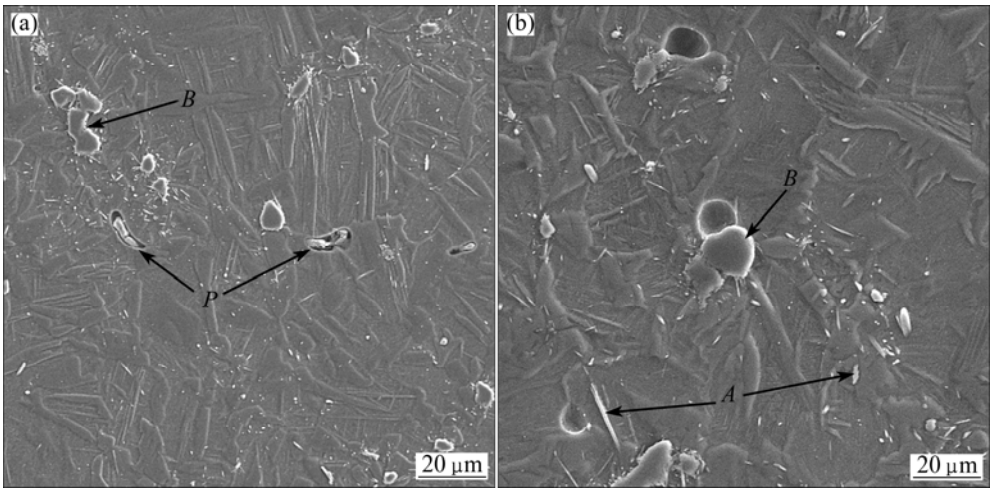

Fig. 6 SEM images of Sample L-SPS2 sintered at 900 °C showing in-situ TiB_w (Points *A*), remained B_4C particles (Point *B*) and porosities (Point *P*)

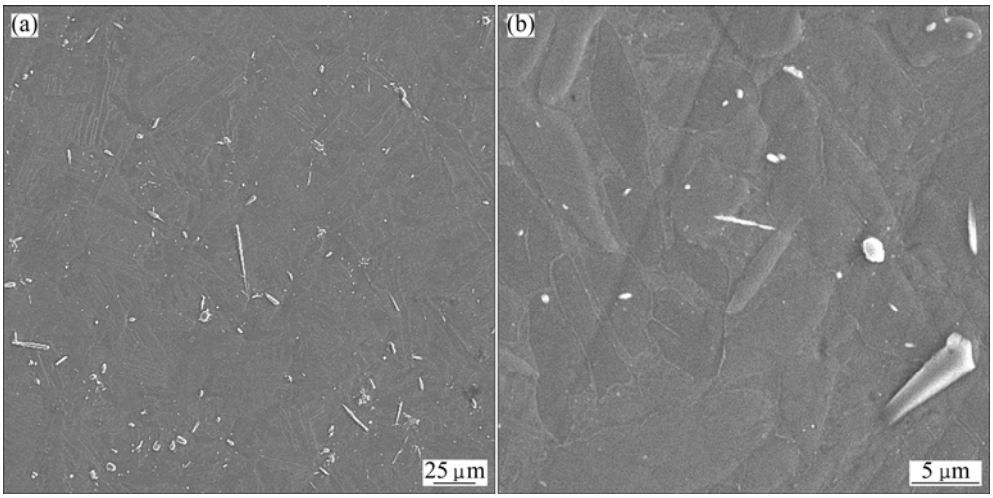

Fig. 7 SEM images of Sample H-SPS2 sintered at 1100 °C showing in-situ TiB_w in matrix free of remained B_4C and porosity

larger. According to the shear-lag model developed for prediction of mechanical properties of discontinuously reinforced metal-matrix composites, the increase in yield strength due to reinforcements is a function of their volume fraction and aspect ratio [32]. Therefore, it can be predicted that the yield strength of SPS samples would be 20% higher than that of the press-and-sintered samples.

The EDS analysis was conducted on 20 different points along a line in Sample L-SPS2 (Fig. 8). The points are located on TiB_w, equiaxed particles and the matrix. The values of Ti and alloying elements Al, V and B are

presented in Fig. 8(b). It is evident that B and Ti contents in the whisker (Point *B*) are 27% and 70%, respectively. EDS analysis of equiaxed particles in Sample L-SPS2 (Points *A* and *C* in Fig. 8) shows that B content reaches about 50%. This confirms that the equiaxed particles in Sample L-SPS2 are the remained B_4C. The chemical composition of the whiskers corresponds to TiB.

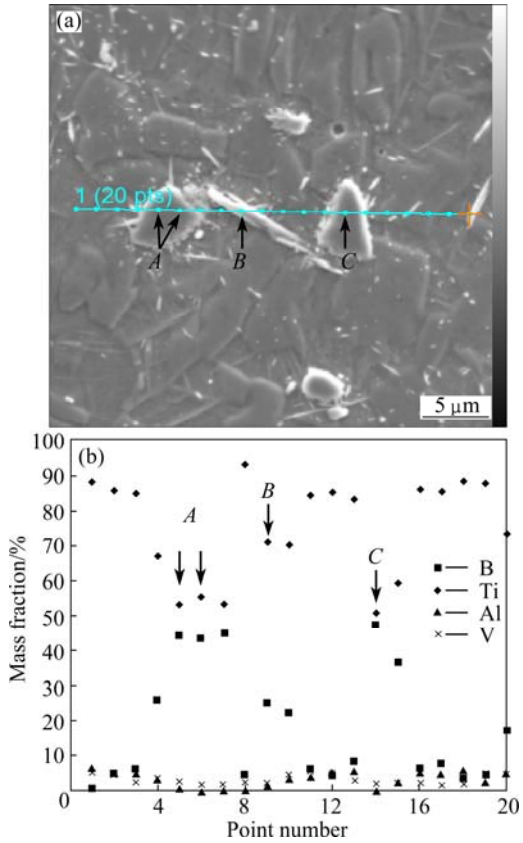

Fig. 8 SEM image of Sample L-SPS2 showing whisker (Point *B*) and cross sections of two particles (Points *A* and *C*) (a) and EDS point analysis results obtained on several consecutive points shown in Fig. 8(a) (b)

One of the defects of the processed composites is the clustering of the in-situ TiB_w. They may be originated by inhomogeneous dispersion of B_4C additives. The results show that the degree of the TiB_w clustering in SPS processed samples is much less than that in the press-and-sintered samples. An occurrence of such defect in Sample L-SPS2 is shown in Fig. 9. It is reported that large size or clustered whiskers would crack at lower strains and alter the deformation properties. Higher diffusion rate in H-SPS samples is the main reason that enhances diffusion of B atoms from the previous B_4C particles. This means the formation of whiskers with higher aspect ratio instead of multiple short TiB_w tangled in some cluster areas. This is in accordance to higher aspect ratio of whiskers in samples processed by SPS (especially H-SPS samples) over those processed by press-and-sintering.

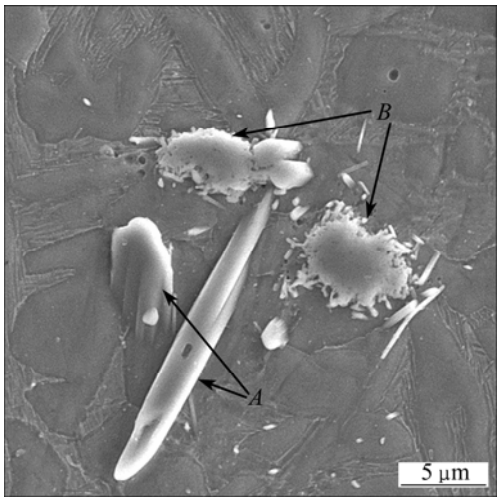

Fig. 9 SEM image of Sample L-SPS2 showing in-situ TiB_w (Points *A*) and two clustered regions of micro-whiskers (Points *B*)

4 Conclusions

1) TMCs were produced by two methods of press-and-sintering and spark plasma sintering.

2) Vacuum sintering of cold pressed samples at 1250 °C for 150 min caused the in-situ formation of TiB_w with the aspect ratio in the range of 8−20 μm. Two main defects of the press-and-sintered samples are the remained porosities and clustering of TiB_w.

3) Although the powder blending parameters remained the same, both of the above mentioned defects were largely restrained by using SPS process. This is mainly due to the simultaneous application of heat and pressure by SPS process.

4) SPS at 1100 °C led to complete reaction of the B_4C additive powder. The microstructural observations revealed that samples produced by SPS at 900 °C contained some un-reacted B_4C particles.

5) The SPS (especially at 1100 °C) process helped to reduce the clustering of TiB whiskers. Increasing the SPS temperature from 900 to 1100 °C also led to the increase of the aspect ratio of TiB_w with whisker length from 7 μm to the range of 10−25 μm. These are interrelated and could be explained by higher diffusion rate provided by simultaneous application of the heat and pressure in SPS process (especially at higher temperature).

References

[1] LIU Y, CHEN L F, TANG H P, LIU C T, LIU B, HUANG B Y. Design of powder metallurgy titanium alloys and composites [J]. Mater Sci Eng A, 2006, 418: 25−35.

[2] LIU Y, LIU Y O, WANG B, QIU J, LIU B, TANG H. Microstructures evolution and mechanical properties of a powder metallurgical titanium alloy with yttrium addition [J]. Mater Manuf Process, 2010,

25: 735−739.

[3] FROES F H. Advances in titanium metal injection molding [J]. Powder Metall Met Ceram, 2007, 46(5−6): 303−310.

[4] NORGATE T E, WELLWOOD G. The potential applications for titanium metal powder and their life cycle impacts [J]. JOM, 2006, 58(9): 58−63.

[5] YUAN Mei-ni, YANG Yan-qing, HUANG Bin, LI Jian-kang, CHEN Yan. Evaluation of interface fracture toughness in SiC fiber reinforced titanium matrix composite [J]. Transactions of Nonferrous Metals Society of China, 2008, 18(4): 925−929.

[6] KAYA F, BOWEN P, LIU J. In-situ observation of crack opening displacement (COD) in a metastable β titanium composite [J]. J Mater Sci, 2008, 43: 270−280.

[7] SELAMAT M S, WATSON L M, BAKER T N. XRD and XPS studies on surface MMC layer of SiC reinforced Ti−6Al−4V alloy [J]. J Mater Process Technol, 2003, 142: 725−737.

[8] MELÉNDEZ I M, NEUBAUER E, DANNINGER H. Consolidation of titanium matrix composites to maximum density by different hot pressing techniques [J]. Mater Sci Eng A, 2010, 527: 4466−4473.

[9] LI S, SUN B, IMAI H, MIMOTO T, KONDOH K. Powder metallurgy titanium matrix composites reinforced with carbon nanotubes and graphite [J]. Compos A: Appl Sci Manuf, 2013, 48: 57−66.

[10] NI D R, GENG L, ZHANG J, ZHENG Z Z. Effect of B_4C particle size on microstructure of in situ titanium matrix composites prepared by reactive processing of Ti−B_4C system [J]. Scripta Mater, 2006, 55: 429−432.

[11] PATEL V V, EL-DESOUKY A, GARAY J E, MORSI K. Pressure-less and current-activated pressure-assisted sintering of titanium dual matrix composites: Effect of reinforcement particle size [J]. Mater Sci Eng A, 2009, 507: 161−166.

[12] WANG M, LU W J, QIN J, MA F, LU J, ZHANG D. Effect of volume fraction of reinforcement on room temperature tensile property of in situ (TiB+TiC)/Ti matrix composites [J]. Mater Des, 2006, 27: 494−498.

[13] LIEBERMAN S I, GOKHALE A M, TAMIRISAKANDALA S, BHAT R B. Three-dimensional microstructural characterization of discontinuously reinforced Ti64−TiB composites produced via blended elemental powder metallurgy [J]. Mater Charact, 2009, 60: 957−963.

[14] LIU B, LIU Y, HE X Y, TANG H P, CHEN L F, HUANG B Y. Preparation and mechanical properties of particulate-reinforced powder metallurgy titanium matrix composites [J]. Metall Mater Trans A, 2007, 38: 2825−2831.

[15] SILVA A A M, SANTOS J F, STROHAECKER T R. An investigation of the fracture behavior of diffusion-bonded Ti6Al4V/TiC/10p [J]. Compos Sci Technol, 2006, 66: 2063−2068.

[16] WANG F, MEI J, WU X. Compositionally graded Ti6Al4V+TiC made by direct laser fabrication using powder and wire [J]. Mater Des, 2007, 28: 2040−2046.

[17] HAN C, LI Y, WU X, REN S, SAN X, ZHU X. Ti/SiO_2 composite fabricated by powder metallurgy for orthopedic implant [J]. Mater Des, 2013, 49: 76−80.

[18] CHOI B J, KIM Y J. In-situ (TiB+TiC) particulate reinforced titanium matrix composites: Effect of B_4C size and content [J]. Met Mater Int, 2013, 19(6): 1301−1307.

[19] NI D R, GENG L, ZHANG J, ZHENG Z Z. Fabrication and tensile properties of in situ TiB_w and TiC_p hybrid-reinforced titanium matrix composites based on Ti−B_4C−C [J]. Mater Sci Eng A, 2008, 478: 291−296.

[20] JEONG H W, KIM S J, HYUN Y T, LEE Y T. Densification and compressive strength of in-situ processed Ti/TiB composites by powder metallurgy [J]. Met Mater Int, 2002, 8(1): 25−35.

[21] WEI S, ZHANG Z, WANG F, SHEN X, CAI H, LEE S, WANG L. Effect of Ti content and sintering temperature on the microstructures and mechanical properties of TiB reinforced titanium composites synthesized by SPS process [J]. Mater Sci Eng A, 2013, 560: 249−255.

[22] TJONG S C, MAI Y W. Processing-structure-property aspects of particulate and whisker-reinforced titanium matrix composites [J]. Compos Sci Technol, 2008, 68: 583−601.

[23] HUANG L J, YANG F Y, HU H T, RONG X D, GENG L, WU L Z. TiB whiskers reinforced high temperature titanium Ti60 alloy composites with novel network microstructure [J]. Mater Des, 2013, 51: 421−426.

[24] MORSI K, PATEL V V, NARAGHI S, GARAY J E. Processing of titanium–titanium boride dual matrix composites [J]. J Mater Process Technol, 2008, 196: 236−242.

[25] QIN L Y, GENG L, NI D. Dry sliding wear behavior of extruded titanium matrix composite reinforced by in situ TiB whisker and TiC particle [J]. J Mater Sci, 2011, 46: 4980−4985.

[26] LU W, ZHANG D, ZHANG X, WU R, SAKATA T, MORI H. Microstructural characterization of TiB in in-situ synthesized titanium matrix composites prepared by common casting technique [J]. J Alloy Compd, 2001, 327: 240−247.

[27] YANG Z, LU W, ZHAO L, LU J, QIN J, ZHANG D. In situ synthesis of hybrid-reinforced titanium matrix composites [J]. Mater Lett, 2007, 61: 2368−2372.

[28] ZHANG Z, LIU Z, LU J, SHEN X, WANG F, WANG Y. The sintering mechanism in spark plasma sintering-proof of the occurrence of spark discharge [J]. Scripta Mater, 2014, 81: 56−59.

[29] ZHANG L, PAN K, WANG J, LIN J. Spark plasma sintering synthesis of intermetallic *T*2 in the Mo−Si−B system [J]. Adv Powder Technol, 2013, 24: 913−920.

[30] FENG H, ZHOU Y, JIA D, MENG Q. Rapid synthesis of Ti alloy with B addition by spark plasma sintering [J]. Mater Sci Eng A, 2005, 390: 344−349.

[31] GORSSE S, MIRACLE D B. Mechanical properties of Ti−6Al−4V/TiB composites with randomly oriented and aligned TiB reinforcements [J]. Acta Mater, 2003, 51: 2427−2442.

[32] KOO M Y, PARK J S, PARK M K, KIM K T, HONG S H. Effect of aspect ratios of in situ formed TiB whiskers on the mechanical properties of TiB_w/Ti−6Al−4V composites [J]. Scripta Mater, 2012, 66: 487−490.

放电等离子烧结法制备原位 TiB 增强 Ti−6Al−4V 复合材料的显微组织特征

Saeid GHESMATI TABRIZI[1], Abolfazl BABAKHANI[1], Seyed Abdolkarim SAJJADI[1], 吕维洁[2]

1. Department of Materials Science and Engineering, Engineering Faculty, Ferdowsi University of Mashhad, Mashhad 9177948974, Iran;
2. 上海交通大学 材料科学与工程学院 金属基复合材料国家重点实验室, 上海 200240

摘 要：钛基复合材料在运输和航空工业领域具有广泛的应用。以 Ti−6Al−4V 和 B_4C 为原料分别采用冷压−真空烧结和放电等离子烧结两种方法制备 TiB 晶须增强钛基复合材料。考察不同复合材料 TiB 晶须的分布、大小以及长径比，研究放电等离子烧结温度对 TiB 晶须增强钛基复合材料的影响。光学显微镜(OM)，扫描电镜(SEM)以及 EDS 分析结果表明：将放电等离子烧结温度从 900 °C 升高到 1100 °C 可以使 TiB 晶须原位自生反应完全，同时减少材料的孔隙含量。

关键词：Ti−6Al−V 金属基复合材料；TiB 晶须；原位反应；放电等离子烧结法

(Edited by Wei-ping CHEN)